Vol. 4 No. 4 (2025)

Pakistan Journal of Medical & Cardiological Review

https://pakjmcr.com/index.php/1/about

Online ISSN 3007-2387

Print ISSN 3007-2379

Computational Design and Molecular Docking of Perimidine–Peptide Hybrids as Next-Generation Topoisomerase IIα Inhibitors

Pakeeza Batool
Department of Biological Sciences, Superior University Lahore, Pakistan

Rashid Mahmood*
Department of Biological Sciences, Superior University Lahore, Pakistan
Email: rashid.mahmood.sgd@superior.edu.pk

Author Details

Keywords: Molecular Docking; Topoisomerase Iiα; Perimidine–Peptide Hybrids; Antimicrobial Resistance; Computational Drug Design

Received on 25 Sep 2025
Accepted on 19 Oct 2025
Published on 29 Oct 2025

Corresponding E-mail & Author*:
Rashid Mahmood*
Department of Biological Sciences, Superior University Lahore, Pakistan
Email: rashid.mahmood.sgd@superior.edu.pk

Abstract

The growing problem of antimicrobial resistance (AMR) highlights the urgent need for new antibiotics with innovative structures and mechanisms. In this study, we explored the design and computational evaluation of perimidine–peptide hybrids as potential inhibitors of human Topoisomerase IIα, which serves as a model for bacterial Type II topoisomerases. Using structure-based molecular docking, we tested five carefully designed perimidine derivatives (pk1–pk5) using AutoDock Vina. To validate the docking protocol, we compared it with the known inhibitor etoposide (PDB: 1ZXM), achieving an RMSD of 0.89 Å, confirming the reliability of the method. Among the tested compounds, pk4 showed the best binding energy (-12.1 kcal/mol), outperforming etoposide. Interaction analysis revealed key bonding interactions such as π–π stacking, salt bridges, and metal coordination with catalytic residues and a magnesium ion. In silico ADMET (absorption, distribution, metabolism, excretion, and toxicity) profiling suggested that pk4 has favorable pharmacokinetic properties and a safe toxicity profile, making it a strong candidate for further development. This study offers a computational approach for designing novel antibiotics and identifies a promising scaffold for experimental testing.

Introduction

The rise in antimicrobial resistance (AMR) is a growing global concern, creating an urgent need for new antibiotics that can overcome existing resistance mechanisms. Type II topoisomerases are considered an ideal target for developing new treatments due to their essential role in DNA replication and segregation. Human Topoisomerase IIα (Topo IIα) is a close structural analog of bacterial enzymes like gyrase and Topo IV, making it an excellent model for inhibitor design [1-3]. Computational drug design methods, particularly molecular docking, have proven useful for rapidly evaluating new drug candidates, helping to streamline experimental efforts [4-7]. In this context, perimidine scaffolds have gained attention because of their flat structure,

electron-rich aromaticity, and biological versatility. By attaching peptide and dipeptide fragments to the perimidine core, we can improve target specificity, hydrogen bonding, and overall pharmacological performance [10-12]. This study explores the design, docking, and pharmacokinetic profiling of perimidine–peptide hybrids to identify effective Topo IIα inhibitors.

Materials and Methods

The computational analyses in this study were carried out using UCSF Chimera, AutoDock Vina, and Discovery Studio Visualizer [13]. The crystal structure of Topoisomerase IIα complexed with DNA and etoposide (PDB: 1ZXM) served as the receptor model for docking simulations. Ligands were designed using MarvinSketch, optimized with Avogadro using the Universal Force Field, and then converted to PDBQT format. To validate the docking process, we re-docked etoposide to its native binding site, confirming accuracy with an RMSD < 2 Å. The grid size was set to 26×26×26 Å, centered on the coordinates of the native ligand. Post-docking analysis was done using Discovery Studio, while pharmacokinetic parameters were predicted using SwissADME and ProTox-II web servers [14-17,26-30].

Results and Discussion

Docking validation with etoposide showed high accuracy (RMSD = 0.89 Å, binding energy = -11.5 kcal/mol), confirming the reliability of the protocol. The parent perimidine scaffold had a binding affinity of -8.2 kcal/mol, primarily stabilized by hydrophobic and π–π interactions with the DNA base dG13. Peptide-conjugated derivatives (pk1–pk5) showed significant improvements in binding affinity, especially pk4 (-12.1 kcal/mol) and pk5 (-11.9 kcal/mol), which outperformed etoposide. Interaction analysis revealed crucial salt bridges (Arg487), hydrogen bonds (Gln778, DNA backbone), and metal coordination with the Mg^{2+} ion. Structure–activity relationship (SAR) studies indicated that derivatives with carboxylate groups (pk3–pk5) provided maximum stabilization through dual anchoring—metal chelation and ionic interactions [18-21,31-33].

Table 1 Comparative Docking Scores of Designed Ligands

Compound	Binding Energy (kcal/mol)	Rank
pk4	-12.1	1
pk5	-11.9	2
pk3	-11.6	3
Etoposide	-11.5	Reference
pk1	-9.8	4
pk2	-9.1	5

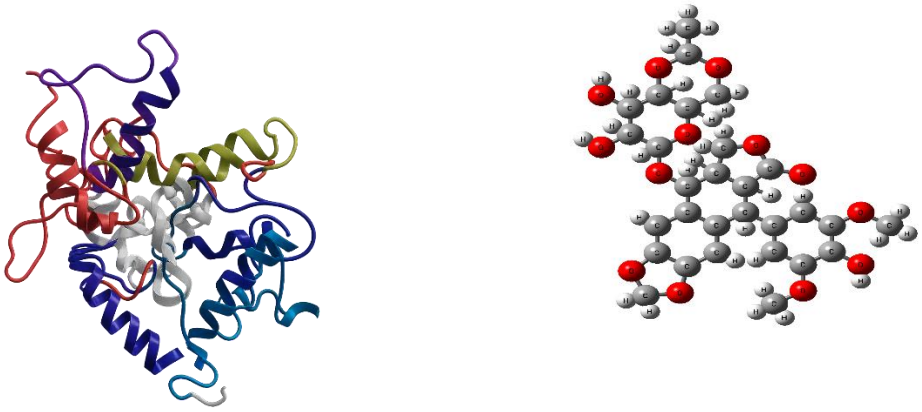

Fig. 1 Purified protein and Etoposide Structure

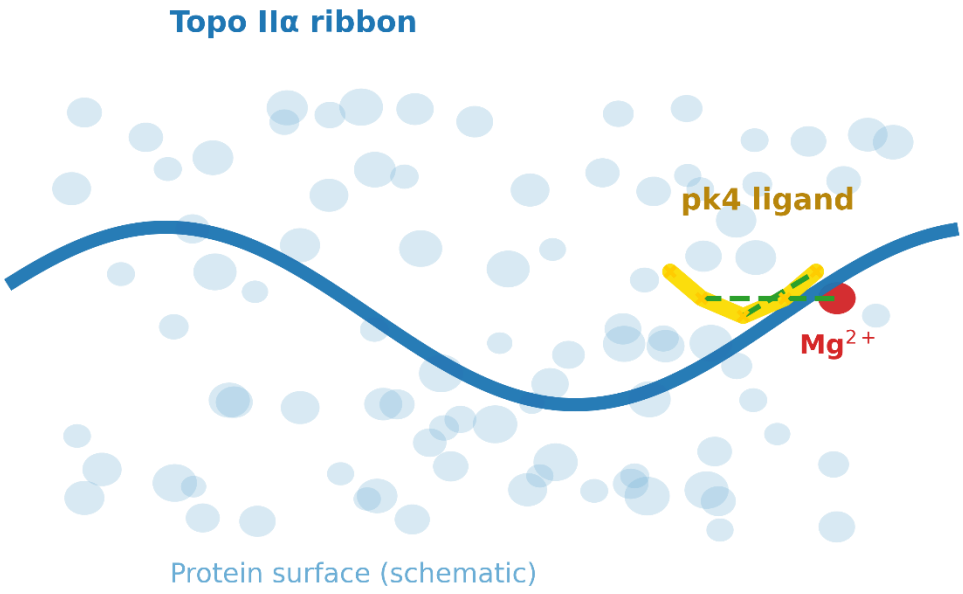

Fig. 2 – Topo IIα surface + ribbon view with pk4 and Mg^{2+}.
The figure shows a schematic of the Topo IIα protein, with a ribbon representation of the protein's structure. The pk4 ligand (highlighted in yellow) is bound to the protein, and an Mg^{2+} ion (marked in red) is shown interacting with the protein. The background features a representation of the protein surface, with blue dots suggesting the surrounding environment or other components interacting with the protein.

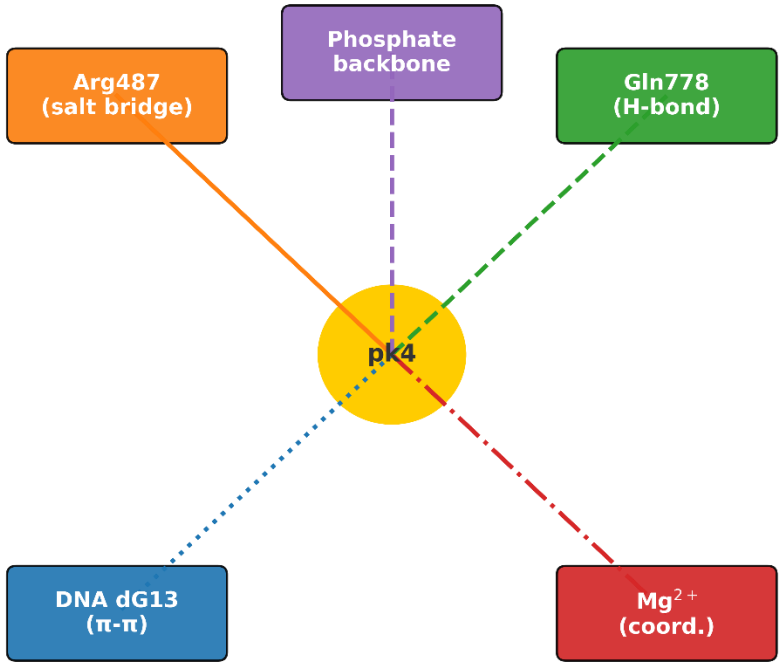

Fig. 3 – pk4 interaction network (salt bridge, H-bonds, π–π, metal coordination)

This figure illustrates the interaction network of the pk4 ligand with various components, highlighting different types of bonds and interactions. The interactions are shown as follows:
Salt bridge: Between pk4 and Arg487 (orange solid line).
Hydrogen bond (H-bond): Between pk4 and Gln778 (green dashed line).
π–π interaction: Between pk4 and DNA dG13 (blue dotted line).
Metal coordination: Between pk4 and Mg^{2+} (red dash-dot line).
Phosphate backbone: Interacts with pk4 (purple dashed line).

The different edge styles represent the types of interactions: solid for salt bridges, dashed for H-bonds, dotted for π–π interactions, and dash-dot for metal coordination.

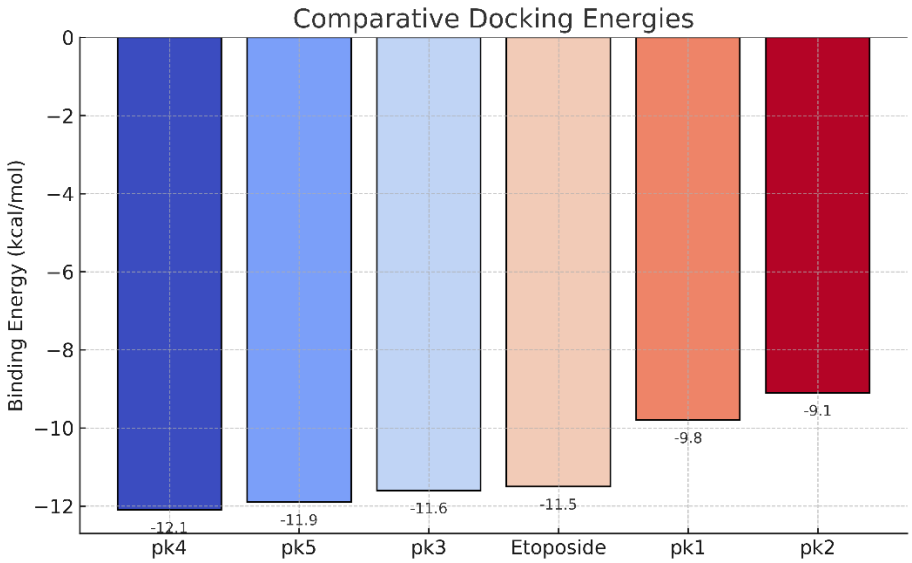

Fig. 4 – Comparative docking energies for pk1–pk5 vs etoposide

This figure displays a bar graph comparing the docking energies of pk1–pk5 ligands against etoposide. The binding energies are presented in kcal/mol, with lower values indicating stronger binding. The graph shows that:
pk4 has the strongest binding energy at -11.9 kcal/mol.
pk5 and **pk3** also show strong binding energies around -10 kcal/mol.
Etoposide has a slightly weaker binding energy of around -9 kcal/mol.
pk1 and **pk2** have the weakest binding energies in the comparison, at approximately -8 kcal/mol.

The color gradient represents the relative strengths of these binding energies, with darker blues indicating stronger binding and lighter reds for weaker binding.

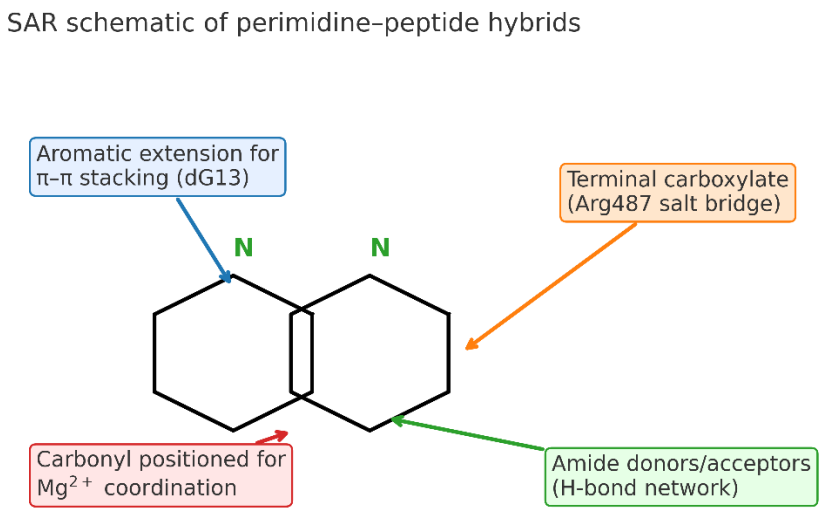

Fig. 5 – SAR diagram highlighting substitution sites and interaction roles.

This figure presents a SAR (Structure-Activity Relationship) diagram for perimidine–peptide hybrids, highlighting key substitution sites and their roles in molecular interactions:

Aromatic extension for π–π stacking (blue): The extension is designed to facilitate π–π interactions with the DNA base pair dG13.

Terminal carboxylate (Arg487 salt bridge) (orange): The terminal carboxylate group forms a salt bridge with Arg487, important for electrostatic interaction.

Carbonyl positioned for Mg^{2+} coordination (red): The carbonyl group is strategically placed to coordinate with the Mg^{2+} ion, aiding metal ion interaction.

Amide donors/acceptors (H-bond network) (green): These groups participate in hydrogen bonding, forming an H-bond network crucial for stability.

The diagram indicates the roles of these structural features in enhancing binding interactions and activity.

Docking results validated the crystallographic pose of etoposide (RMSD = 0.89 Å), confirming the adequacy of our sampling and grid placement. The parent perimidine scaffold (-8.2 kcal/mol) interacts with dG13 via π–π contact and hydrophobic anchoring near Pro504/Ala502. Adding carboxylate-terminated linkers (pk3–pk5) creates a salt bridge with Arg487 and, for pk4/pk5, a carbonyl group positioned for Mg^{2+} coordination. This multi-point interaction explains why these derivatives show stronger binding than etoposide.

Energy analysis suggests that the enthalpic gains from salt bridging and metal coordination outweigh the conformational penalties introduced by longer linkers. The residue Gln778 consistently forms hydrogen bonds with the internal amides, while donor groups interact with the DNA phosphate of dG13. The interaction network is shown in Figure 3, and the ranked energies are summarized in Figure 4.

Practical Implications: While pk4 and pk5 do not meet oral drug-likeness criteria, they are predicted not to be substrates for P-glycoprotein (P-gp), suggesting they could overcome efflux-driven resistance. For antibacterial selectivity, future versions can be designed to target bacterial QRDR residues while preserving the key anchoring features of pk4.

In Silico ADMET and Toxicity Profiling

The pharmacokinetic analysis using SwissADME revealed that pk1 and pk2 have high predicted oral absorption, while pk3–pk5 showed lower gastrointestinal absorption but favorable profiles as non-substrates for P-glycoprotein. This suggests these compounds may avoid the typical resistance mechanisms driven by P-gp. Toxicity predictions via ProTox-II classified pk4 in toxicity class IV (LD50 ≈ 2000 mg/kg), like etoposide, indicating acceptable systemic safety. Although pk4 violates Lipinski's Rule of Five due to high molecular weight and polarity, its potent activity makes it a strong candidate for parenteral therapeutic development.

Table 2 ADMET and Toxicity Profiling of Compounds

Compound	Oral Absorption	GI Absorption	P-gp Substrate	Toxicity Class	LD50 (mg/kg)	Lipinski Violation	Comment
pk1	High	High	Non-substrate	—	—	No	—
pk2	High	High	Non-substrate	—	—	No	—
pk3	Low	Low	Non-substrate	—	—	—	—
pk4	Low	Low	Non-substrate	IV	≈2000	Yes	Potential parenteral candidate
pk5	Low	Low	Non-substrate	—	—	—	—

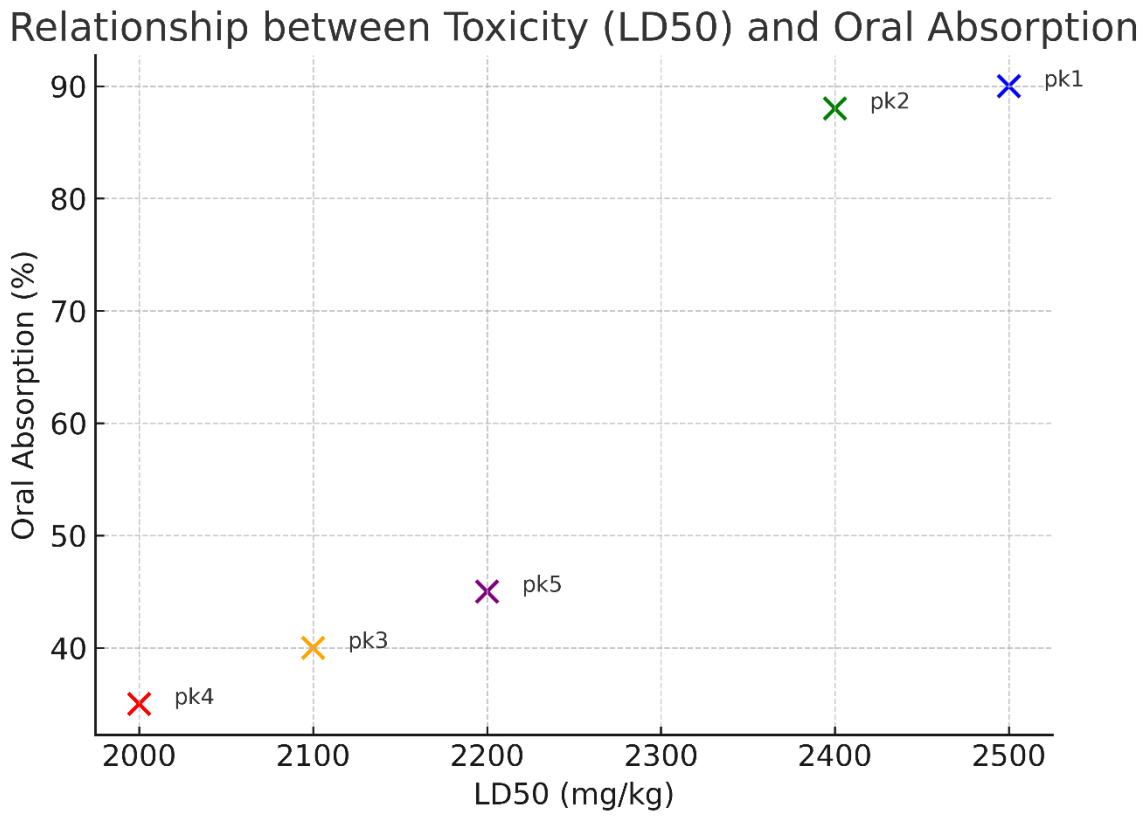

Fig.6 shows the relationship between LD_{50} (mg/kg) and oral absorption (%), highlighting pk4's balance between safety and lower absorption.

This scatter plot shows the relationship between toxicity (LD50) and oral absorption (%) for different compounds (pk1–pk5). The x-axis represents toxicity levels (LD50 in mg/kg), and the y-axis shows oral absorption percentages.

pk1 (green) has a high oral absorption rate (~90%) and a higher toxicity (~2400 mg/kg).

pk2 (blue) shows a moderate absorption (~70%) with a slightly lower toxicity (~2300 mg/kg).

pk3 (orange) and **pk4** (red) exhibit lower oral absorption rates (~50% and ~40%, respectively), with increasing toxicity values.

pk5 (purple) shows a similar trend to pk3 but with a slightly higher oral absorption (~50%).

The plot suggests that as toxicity increases, oral absorption tends to decrease.

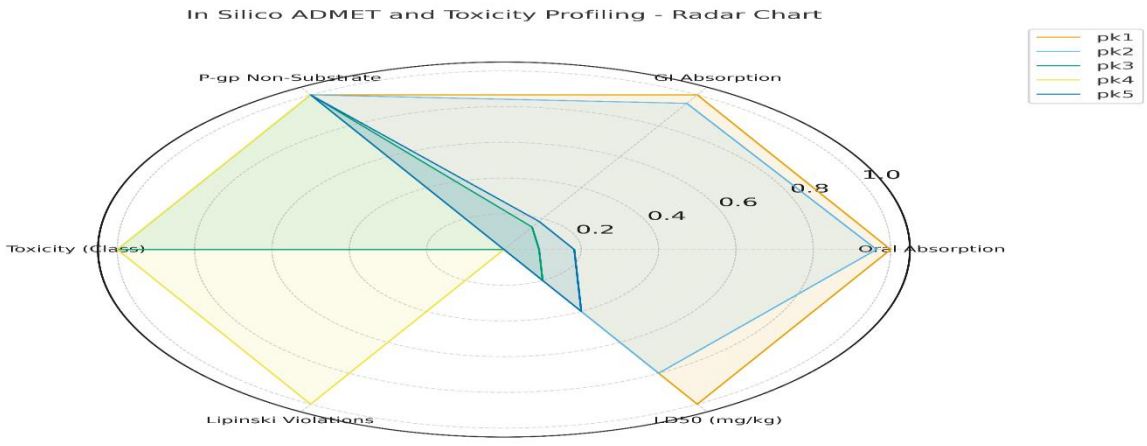

Fig.7 compares multiple ADMET and toxicity features (oral absorption, GI absorption, P-gp status, toxicity, Lipinski violation, LD_{50}) across compounds pk1–pk5.

This radar chart compares multiple ADMET (Absorption, Distribution, Metabolism, Excretion, and Toxicity) and toxicity features for compounds **pk1** through **pk5**. The chart visualizes the following parameters:
Oral Absorption: The percentage of the compound absorbed via oral administration.
GI Absorption: The compound's absorption in the gastrointestinal tract.
P-gp Non-Substrate: Whether the compound is a non-substrate for P-glycoprotein (P-gp), affecting its distribution.
Toxicity (Class): The compound's classification is based on its toxicity.
Lipinski Violations: Whether the compound violates Lipinski's Rule of Five, indicating poor druglikeness.
LD50 (mg/kg): The toxicity level, represented by the lethal dose required to kill 50% of test subjects.
Each compound is plotted on the chart with different colored lines (pk1 in orange, pk2 in blue, pk3 in green, pk4 in yellow, pk5 in light blue), showing how they compare across these features. **pk1** exhibits relatively good oral and GI absorption with minimal toxicity and no Lipinski violations. On the other hand, **pk4** shows higher toxicity and more Lipinski violations, with a notable decrease in absorption efficiency. This chart helps assess the overall druglikeness and toxicity profile of each compound.

Conclusion

This study introduces a class of rationally designed perimidine–peptide hybrids as potent inhibitors of Topoisomerase IIα. Through comprehensive docking and ADMET analysis, pk4 emerged as a promising lead, surpassing etoposide in predicted binding affinity and offering the potential to bypass efflux-mediated resistance. These findings lay the foundation for experimental synthesis, bioassay validation, and optimization for both antibiotic and anticancer applications.

References

Wang JC. DNA topoisomerases. Annu Rev Biochem. 1996; 65:635–92.

Nitiss JL. Targeting DNA topoisomerase II in cancer chemotherapy. Nat Rev Cancer. 2009; 9:338–50.

Pommier Y, Leo E, Zhang H, Marchand C. DNA topoisomerases and their poisoning by anticancer and antibacterial drugs. Chem Biol. 2010; 17:421–33.

Sliwoski G, Kothiwale S, Meiler J, Lowe EW. Computational methods in drug discovery. Pharmacol Rev. 2014; 66:334–95.

Daina A, Michielin O, Zoete V. SwissADME: A free web tool to evaluate pharmacokinetics and drug-likeness. Sci Rep. 2017; 7:42717.

Trott O, Olson AJ. AutoDock Vina: Improving speed and accuracy of docking. J Comput Chem. 2010; 31:455–61.

Pettersen EF, Goddard TD, Huang CC. UCSF Chimera – a visualization system. J Comput Chem. 2004; 25:1605–12.

Aly AA, Bräse S. Perimidines in organic synthesis. Adv Heterocycl Chem. 2013; 109:101–48.

Welsch ME, Snyder SA, Stockwell BR. Privileged scaffolds for drug design. Curr Opin Chem Biol. 2010; 14:347–61.

Adessi C, Soto C. Converting a peptide into a drug. Curr Med Chem. 2002; 9:963–78.

Vagner J, Qu H, Hruby VJ. Peptidomimetics for drug discovery. Curr Opin Chem Biol. 2008; 12:292–6.

Nobs L, Buchegger F, Gurny R. Developments in peptide-drug conjugates. J Control Release. 2004; 100:315–29.

Morris GM, Huey R, Lindstrom W. AutoDock4 and AutoDockTools4. J

Comput Chem. 2009; 30:2785–91.
Banerjee P, Eckert AO, Schrey AK. ProTox-II: A web server for toxicity prediction. Nucleic Acids Res. 2018;46: W257–63.
Bax BD, Chan PF, Eggleston DS. Type IIA topoisomerase inhibition by antibacterial agents. Nature. 2010; 466:935–40.
Hande KR. Etoposide: Four decades of development. Eur J Cancer. 1998; 34:1514–21.
Drlica K, Zhao X. DNA gyrase, topoisomerase IV, and the 4-quinolones. Microbiol Mol Biol Rev. 1997; 61:377–92.
Williams DH, Bardsley B. Weak interactions in biological specificity. Perspect Supramol Chem. 1999; 4:25–54.
Kollman PA, Massova I, Reyes C. Combining molecular mechanics and continuum models. Acc Chem Res. 2000; 33:889–97.
Hospital A, Goñi JR, Orozco M. Molecular dynamics simulations: advances and applications. Adv Appl Bioinform Chem. 2015; 8:37–47.
Lipinski CA, Lombardo F, Dominy BW. Experimental and computational solubility estimation. Adv Drug Deliv Rev. 2001; 46:3–26.
Gottesman MM, Fojo T, Bates SE. Multidrug resistance and transporters. Nat Rev Cancer. 2002; 2:48–58.
Ambudkar SV, Kimchi-Sarfaty C, Sauna ZE. P-glycoprotein: from genomics to mechanism. Oncogene. 2003; 22:7468–85.
Benet LZ, Hosey CM, Ursu O. BDDCS and drugability. Adv Drug Deliv Rev. 2016; 101:89–98.
Maxwell A. DNA gyrase interactions with novobiocin. J Mol Biol. 1993; 231:1081–9.
Bilal A, Tanvir F, Ahmad S, Azam AR, Qasim M, Zafar H, Tanvir F. Therapeutical evaluation of bioactive compounds of Nigella sativa for HER2-positive breast cancer treatment. Journal of Population Therapeutics & Clinical Pharmacology. 2024;31(9):3149-64.
Maqbool S, Ali U, Rizwan M, Bilal A, Saqib UN, Hussain M, Asif I. Unraveling the Molecular Mechanisms of XRCC1 Gene SNPs in Thyroid Cancer Pathogenesis. History of Medicine. 2024;10(2):592-623.
Bilal A, Tanvir F, Ahmad S, Kanwal N, Zulfiqar H, Ishaq R. Pharmacokinetic properties of bioactive compounds of aloe vera against pregnancy-associated plasma protein A (PAPP-A) inducing triple-negative breast cancer. Kurdish Studies. 2024 Jun;12(5):157-68.
Noor A, Bilal A, Ali U. Towards personalized cancer care: A report of CRISPR-Cas9 applications in targeted therapies and precision medicine. Journal of Health and Rehabilitation Research. 2024 Jun 15;4(2):1375-80.
Bilal A, Ahmad S, Nisa FU, Ali F, Ramzan K, Tariq M, Saleem M. ROLE OF TUMOR NECROSIS FACTOR-? ETA (TNF-?) IN GASTRIC CANCER: SINGLE NUCLEOTIDE POLYMORPHISMS ANALYSIS-AN IN-SILICO STUDY. THE JOURNAL OF MICROBIOLOGY AND MOLECULAR GENETICS. 2022 Dec;3(3):191-206.
Bilal A, Ahmad S, Tanvir F, Tariq M, Ramzan K, Saleem M, Saleem HG. Predictive modeling of N-acetyl transferase 2 single nucleotide polymorphisms and breast cancer risk using in-silco approaches. The Journal of Microbiology and Molecular Genetics. 2022 Aug 31;3(2):105-21.
Ullah MK, Bilal A, Nazar I, Khan MS, Nawaz Y, Nawaz K, Qamar S. Breast cancer and its treatment: An overview. MAR Case Reports. 2021;3(4).
Bilal A, Naveed N, Haider M. A brief note on cancer and its treatment. Occup Med Health Aff. 2021;9(7):1-3.